High-resolution fiber optic microscopy with fluorescent contrast enhancement for the identification of axillary lymph node metastases in breast cancer: a pilot study

Kelsey J. Rosbach,[1,*] Dongsuk Shin,[1] Timothy J. Muldoon,[1] Mohammad A. Quraishi,[2] Lavinia P. Middleton,[3] Kelly K. Hunt,[4] Funda Meric-Bernstam,[4] Tse-Kuan Yu,[5] Rebecca R. Richards-Kortum,[1] and Wei Yang[2]

[1]*Department of Bioengineering, Rice University, 6100 Main Street, Houston, Texas 77005, USA*
[2]*Department of Diagnostic Radiology, The University of Texas M. D. Anderson Cancer Center, 1515 Holcombe Boulevard, Houston, Texas 77030, USA*
[3]*Department of Pathology, The University of Texas M. D. Anderson Cancer Center, 1515 Holcombe Boulevard, Houston, Texas 77030, USA*
[4]*Department of Surgical Oncology, The University of Texas M. D. Anderson Cancer Center, 1515 Holcombe Boulevard, Houston, Texas 77030, USA*
[5]*Department of Radiation Oncology, The University of Texas M. D. Anderson Cancer Center, 1515 Holcombe Boulevard, Houston, Texas 77030, USA*
**kelsey.rosbach@gmail.com*

Abstract: This prospective pilot study evaluates the potential of high-resolution fiber optic microscopy (HRFM) to identify lymph node metastases in breast cancer patients. 43 lymph nodes were collected from 14 consenting breast cancer patients. Proflavine dye was topically applied to lymph nodes *ex vivo* to allow visualization of nuclei. 242 images were collected at 105 sites with confirmed histopathologic diagnosis. Quantitative statistical features were calculated from images, assessed with one-way ANOVA, and were used to develop a classification algorithm with the goal of objectively discriminating between normal and metastatic tissue. A classification algorithm using mean image intensity and skewness achieved sensitivity of 79% (27/34) and specificity of 77% (55/71). This study demonstrates the technical feasibility and diagnostic potential of HRFM with fluorescent contrast in the *ex vivo* evaluation of lymph nodes from breast cancer patients.

OCIS codes: (170.1610) Clinical applications; (170.6935) Tissue characterization.

References and links

1. U. S. Cancer Statistics Working Group, "United States Cancer Statistics: 1999–2005 Incidence and Mortality Web-based Report," Atlanta: U.S. Department of Health and Human Services, Centers for Disease Control and Prevention and National Cancer Institute, 2009, *www.cdc.gov/uscs*.
2. M. Duff, A. D. Hill, G. McGreal, S. Walsh, E. W. McDermott, and N. J. O'Higgins, "Prospective evaluation of the morbidity of axillary clearance for breast cancer," Br. J. Surg. **88**(1), 114–117 (2001).
3. R. J. Kennedy, J. Bradley, R. W. Parks, and S. J. Kirk, "Prospective evaluation of the morbidity of axillary clearance for breast cancer (Br J Surg 2001; 88: 114-7)," Br. J. Surg. **88**(6), 891 (2001).
4. W. Kwan, J. Jackson, L. M. Weir, C. Dingee, G. McGregor, and I. A. Olivotto, "Chronic arm morbidity after curative breast cancer treatment: prevalence and impact on quality of life," J. Clin. Oncol. **20**(20), 4242–4248 (2002).
5. J. Engel, J. Kerr, A. Schlesinger-Raab, H. Sauer, and D. Hölzel, "Axilla surgery severely affects quality of life: results of a 5-year prospective study in breast cancer patients," Breast Cancer Res. Treat. **79**(1), 47–57 (2003).
6. S. A. Norman, A. R. Localio, S. L. Potashnik, H. A. Simoes Torpey, M. J. Kallan, A. L. Weber, L. T. Miller, A. Demichele, and L. J. Solin, "Lymphedema in breast cancer survivors: incidence, degree, time course, treatment, and symptoms," J. Clin. Oncol. **27**(3), 390–397 (2008).
7. J. J. Albertini, G. H. Lyman, C. Cox, T. Yeatman, L. Balducci, N. Ku, S. Shivers, C. Berman, K. Wells, D. Rapaport, A. Shons, J. Horton, H. Greenberg, S. Nicosia, R. Clark, A. Cantor, and D. S. Reintgen, "Lymphatic mapping and sentinel node biopsy in the patient with breast cancer," JAMA **276**(22), 1818–1822 (1996).

#132359 - $15.00 USD Received 30 Jul 2010; revised 11 Sep 2010; accepted 11 Sep 2010; published 16 Sep 2010

8. D. Krag, D. Weaver, T. Ashikaga, F. Moffat, V. S. Klimberg, C. Shriver, S. Feldman, R. Kusminsky, M. Gadd, J. Kuhn, S. Harlow, P. Beitsch, P. Whitworth, Jr., R. Foster, Jr., and K. Dowlatshahi, "The sentinel node in breast cancer--a multicenter validation study," N. Engl. J. Med. **339**(14), 941–946 (1998).
9. K. M. McMasters, A. E. Giuliano, M. I. Ross, D. S. Reintgen, K. K. Hunt, D. R. Byrd, V. S. Klimberg, P. W. Whitworth, L. C. Tafra, and M. J. Edwards, "Sentinel-lymph-node biopsy for breast cancer--not yet the standard of care," N. Engl. J. Med. **339**(14), 990–995 (1998).
10. R. K. Orr, J. L. Hoehn, and N. F. Col, "The learning curve for sentinel node biopsy in breast cancer: practical considerations," Arch. Surg. **134**(7), 764–767 (1999).
11. U. Veronesi, G. Paganelli, V. Galimberti, G. Viale, S. Zurrida, M. Bedoni, A. Costa, C. de Cicco, J. G. Geraghty, A. Luini, V. Sacchini, and P. Veronesi, "Sentinel-node biopsy to avoid axillary dissection in breast cancer with clinically negative lymph-nodes," Lancet **349**(9069), 1864–1867 (1997).
12. U. Veronesi, G. Paganelli, G. Viale, V. Galimberti, A. Luini, S. Zurrida, C. Robertson, V. Sacchini, P. Veronesi, E. Orvieto, C. De Cicco, M. Intra, G. Tosi, and D. Scarpa, "Sentinel lymph node biopsy and axillary dissection in breast cancer: results in a large series," J. Natl. Cancer Inst. **91**(4), 368–373 (1999).
13. A. Lee, S. Krishnamurthy, A. Sahin, W. F. Symmans, K. Hunt, and N. Sneige, "Intraoperative touch imprint of sentinel lymph nodes in breast carcinoma patients," Cancer **96**(4), 225–231 (2002).
14. A. F. Gmitro, and D. Aziz, "Confocal microscopy through a fiber-optic imaging bundle," Opt. Lett. **18**(8), 565 (1993).
15. R. F. Hwang, S. Krishnamurthy, K. K. Hunt, N. Mirza, F. C. Ames, B. Feig, H. M. Kuerer, S. E. Singletary, G. Babiera, F. Meric, J. S. Akins, J. Neely, and M. I. Ross, "Clinicopathologic factors predicting involvement of nonsentinel axillary nodes in women with breast cancer," Ann. Surg. Oncol. **10**(3), 248–254 (2003).
16. B. A. Flusberg, E. D. Cocker, W. Piyawattanametha, J. C. Jung, E. L. Cheung, and M. J. Schnitzer, "Fiber-optic fluorescence imaging," Nat. Methods **2**(12), 941–950 (2005).
17. L. R. Ferguson, and W. A. Denny, "The genetic toxicology of acridines," Mutat. Res. **258**(2), 123–160 (1991).
18. T. J. Muldoon, M. C. Pierce, D. L. Nida, M. D. Williams, A. Gillenwater, and R. Richards-Kortum, "Subcellular-resolution molecular imaging within living tissue by fiber microendoscopy," Opt. Express **15**(25), 16413–16423 (2007).
19. T. J. Muldoon, S. Anandasabapathy, D. Maru, and R. Richards-Kortum, "High-resolution imaging in Barrett's esophagus: a novel, low-cost endoscopic microscope," Gastrointest. Endosc. **68**(4), 737–744 (2008).
20. D. W. Edlow, and D. Carter, "Heterotopic epithelium in axillary lymph nodes: report of a case and review of the literature," Am. J. Clin. Pathol. **59**(5), 666–673 (1973).
21. S. Alvarez, E. Añorbe, P. Alcorta, F. López, I. Alonso, and J. Cortés, "Role of sonography in the diagnosis of axillary lymph node metastases in breast cancer: a systematic review," AJR Am. J. Roentgenol. **186**(5), 1342–1348 (2006).
22. M. de Boer, J. A. van Dijck, P. Bult, G. F. Borm, and V. C. Tjan-Heijnen, "Breast cancer prognosis and occult lymph node metastases, isolated tumor cells, and micrometastases," J. Natl. Cancer Inst. **102**(6), 410–425 (2010).
23. P. Gimbergues, M. M. Dauplat, X. Durando, C. Abrial, G. Bouedec, M. A. Mouret-Reynier, F. Cachin, F. Kwiatkowski, A. Tchirkov, J. Dauplat, and F. Penault-Llorca, "Intraoperative imprint cytology examination of sentinel lymph nodes after neoadjuvant chemotherapy in breast cancer patients," Ann. Surg. Oncol. **17**(8), 2132–2137 (2010).
24. F. Crippa, A. Gerali, A. Alessi, R. Agresti, and E. Bombardieri, "FDG-PET for axillary lymph node staging in primary breast cancer," Eur. J. Nucl. Med. Mol. Imaging **31**(0 Suppl 1), S97–S102 (2004).
25. M. Pramanik, K. H. Song, M. Swierczewska, D. Green, B. Sitharaman, and L. V. Wang, "In vivo carbon nanotube-enhanced non-invasive photoacoustic mapping of the sentinel lymph node," Phys. Med. Biol. **54**(11), 3291–3301 (2009).
26. K. H. Song, C. Kim, K. Maslov, and L. V. Wang, "Noninvasive in vivo spectroscopic nanorod-contrast photoacoustic mapping of sentinel lymph nodes," Eur. J. Radiol. **70**(2), 227–231 (2009).
27. J. C. Boughey, J. P. Moriarty, A. C. Degnim, M. S. Gregg, J. S. Egginton, and K. H. Long, "Cost modeling of preoperative axillary ultrasound and fine-needle aspiration to guide surgery for invasive breast cancer," Ann. Surg. Oncol. **17**(4), 953–958 (2010).

1. Introduction

Breast cancer is the most common malignancy affecting women in North America and Europe, with approximately 200,000 new cases treated each year in the United States alone [1]. Treatment that involves surgical resection of the primary tumor often includes removal of axillary lymph nodes. The presence of axillary lymph node metastases is the most important prognostic factor for the patient, and determines appropriate adjuvant therapy after surgery [2]. However, axillary dissection is associated with significant short-term and long-term complications including lymphedema and upper extremity dysfunction in up to 50% of patients [3–6]. Identification and subsequent removal and assessment of the sentinel lymph node (SLN) has emerged as an alternative to full axillary dissection. This procedure has fewer complications than axillary dissection, however, there is potential for false negative events in 10-15% of patients [7–12]. This could result in understaging, which impacts adjuvant therapy recommendations, and the potential for regional recurrence in the axilla. An additional

#132359 - $15.00 USD Received 30 Jul 2010; revised 11 Sep 2010; accepted 11 Sep 2010; published 16 Sep 2010

challenge for clinicians is the fact that touch imprint cytological analysis at the time of SLN surgery only identifies the presence of metastases in 50-80% of patients who have lymph node metastases [13]. A second surgical procedure is required when SLN metastases are identified on permanent histologic analysis in up to 35% of patients [14]. Therefore, additional methods to detect lymph node metastases intra-operatively have the potential to identify appropriate candidates for axillary dissection and avoid false negative events. Other clinical situations in which additional methods to detect lymph node metastases would be useful include patients with ductal carcinoma in situ for whom operative removal of the SLN remains controversial or for pre-treatment staging of the axilla in patients who are candidates for neoadjuvant chemo- and endocrine therapy.

Current diagnostic approaches rely on optical imaging of stained cytological or histological specimens. Recent advances in optical imaging and optically active contrast agents allow high-resolution imaging of cell morphology and tissue architecture *in vivo* without the need for resection [15,16]. High-resolution fiber optic microscopy (HRFM) is a new imaging technology that when used together with a fluorescent contrast agent, enables real time visualization of tissue with sub-cellular resolution *in vivo*. Proflavine is a fluorescent dye that stains nuclei [17]. HRFM with proflavine application has been investigated as a diagnostic tool to distinguish benign from malignant tissue in the oral cavity and esophagus [18,19]. HRFM with proflavine staining has the potential to image cellular morphologic changes that are critical in the pathologic evaluation of lymph node metastases by exploiting the cell/nucleus size difference between carcinoma and lymphoid cells. Traditional histopathological analysis of lymph nodes in breast cancer patients identifies epithelial cell clusters, which are enlarged and crowded compared to normal lymphocytes, are hyperchromatic with hematoxylin and eosin (H&E) staining, and have an increased nuclear to cytoplasmic ratio [20]. In patients who have received preoperative chemotherapy, lymph nodes can contain stromal fibrosis and individual tumor cells may be embedded within the fibrosis.

The goal of this prospective study was to evaluate the potential of HRFM with proflavine staining for the detection of lymph node metastases in breast cancer patients. While this study was performed *ex vivo* as a proof of concept, HRFM with proflavine staining may eventually be performed *in vivo* and thus could play an important role in clinical management of breast cancer patients, particularly for intra-operative assessment of lymph nodes in patients with early disease or for pre-treatment staging of the axilla.

2. Methods

The high-resolution microendoscope has previously been described in detail [18]. The HRFM instrument uses a light emitting diode (LED) with excitation light centered at 455 nm to excite proflavine fluorescence. A fiber-optic bundle composed of 30,000 fibers with a center-to-center spacing of approximately four μm transmits the light and is placed in direct contact with the surface to be imaged. The field of view comprises a circle that measures 750 μm in diameter. The system achieves a lateral resolution of 4.4 μm, sufficient to resolve individual cell nuclei. Figure 1 shows an optical diagram of the battery-powered HRFM instrument along with a photograph demonstrating the small size and portability of the instrument. The system can be assembled for $4,500.

#132359 - $15.00 USD Received 30 Jul 2010; revised 11 Sep 2010; accepted 11 Sep 2010; published 16 Sep 2010

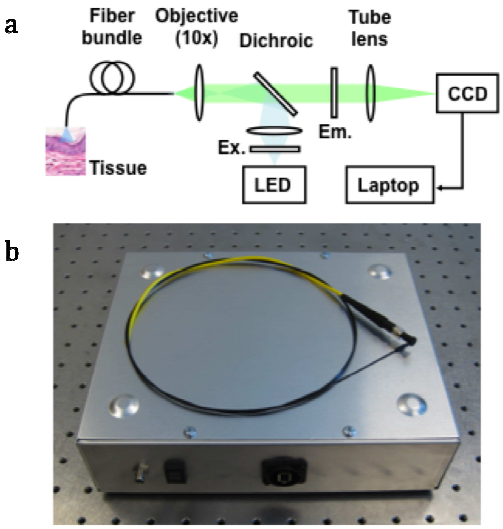

Fig. 1. (a) Optical diagram of the high-resolution microendoscope (b) Photograph demonstrating the small size and portability of the battery-powered instrument.

2.1 Clinical study

Women 18 and older undergoing surgery for breast cancer that included a SLN biopsy followed by complete axillary lymph node dissection were eligible to participate in this study. Patients enrolled in this study gave written informed consent to participate, and the study was reviewed and approved by the institutional review boards at two academic institutions. To comply with HIPAA policies, patient data were labeled by accrual number.

Three to four representative fresh lymph node specimens were taken from each patient and prepared for imaging. To ensure that images were taken of areas representing normal lymphoid tissue and tumor metastases, a dedicated breast pathologist selected one lymph node that was grossly normal and one lymph node that showed gross metastasis. Other lymph nodes selected for imaging were grossly ambiguous. For some patients, all the lymph nodes appeared normal; in these cases three normal appearing nodes were imaged. A dedicated breast pathologist bisected each node to facilitate lymphoid tissue imaging.

Each lymph node was photographed and imaging sites were marked on the photograph to serve as reference points for histopathological correlation. A 0.01% solution (w/v) of proflavine hydrochloride (Sigma-Aldrich Corp., St. Louis, MO) was topically applied to the cut surface of the lymph nodes for approximately ten seconds. The fiber bundle of the HRFM instrument was placed in direct contact with the surface of the node for imaging. Multiple images were acquired from adjacent fields of view at each location on the specimen by translating the probe position approximately 1 mm. On average, three nodes could be imaged at approximately ten sites within ten to fifteen minutes. Following imaging, the nodes were submitted for routine processing and H&E staining in specially labeled cassettes to facilitate direct imaging–histopathological correlation. A dedicated breast pathologist reviewed the axillary lymph nodes for metastases, and the final histopathological diagnosis was used as the gold standard for each imaging site. Imaging sites with unequivocal histopathological correlation were included in further analysis.

2.2 Image analysis

Each image was reviewed to determine that quality control criteria were met. Images with motion artifacts or inadequate contact between fiber bundle and tissue were excluded from analysis. Each image that passed quality control was analyzed to identify quantitative features that could be useful to distinguish normal lymphoid tissue from metastases. Because adipose

#132359 - $15.00 USD Received 30 Jul 2010; revised 11 Sep 2010; accepted 11 Sep 2010; published 16 Sep 2010

tissue is not useful in this distinction, all images were first cropped to remove regions of adipocytes and obtain a rectangular shaped field containing nuclei of lymphocytes or tumor cells. The dimensions of this field were variable because the region of each image containing nuclei of interest was also variable. A reference standard (captured in each image) was used to normalize pixel intensity values of the green channel of each corresponding image to account for any potential day-to-day variation in the HRFM instrument and to allow comparison between images with different exposure times.

Five image features were calculated from each normalized region (Matlab, Mathworks, CA). These features included: mean image intensity, standard deviation of image intensity, skewness, kurtosis, and entropy. Mean image intensity was selected as a feature that may be useful to separate normal lymphoid tissue from metastatic tissue because malignant cells crowd together, are enlarged, and are hyperchromatic with H&E stain. Since proflavine stains nuclei, images containing malignant cells may have a higher intensity than images of normal lymphatic tissue. The remaining four features describe variations in pixel intensity throughout the image and were evaluated because the disruption of tissue architecture that occurs with metastasis may also alter the distribution of pixel intensity values. Standard deviation describes the spread of pixel values relative to the mean; high values of standard deviation correspond to a wider image histogram with a wide range of pixel intensities. Skewness describes asymmetry of the image histogram and indicates if pixel values are concentrated at low or high values. Positive skewness on a histogram occurs when there are more low values than high, negative skewness when there is a concentration on high values, and zero skewness describes a symmetric histogram. Kurtosis describes the peakedness of an image histogram and is sensitive to the size of the histogram tails. Entropy is a statistical measure of randomness that can be used to characterize the texture of an image. High values of entropy indicate greater randomness while low values of entropy result from a more uniform image. Each of these investigated features represents an objective, quantitative metric for assessing pixel intensity and distribution in an image.

Since multiple images of adjacent fields of view were obtained at each site in order to increase the region surveyed, the feature values calculated for each image were grouped by site and then averaged. A one-way ANOVA test was performed to compare average feature values from sites containing normal lymphoid tissue and sites containing metastases. For each feature, a classification algorithm was developed using linear discriminant analysis to discriminate between normal lymphoid tissue and lymph nodes containing metastases, using histology as the gold standard. Because this was a pilot study with a relatively small number of measurements, the same data set was used to train the algorithm and test its performance. Sensitivity and specificity of classification were calculated for each of the five features. A receiver operator characteristic (ROC) curve was constructed and the area under the curve (AUC) was recorded. The two features with the best individual diagnostic performance were identified, and classification performance was also assessed when these two features were used together.

3. Results

A total of 43 lymph nodes were collected from 14 patients for imaging with HRFM; 13 patients had three nodes imaged and one had four nodes imaged. Of the 43 lymph nodes, 27 were normal and 16 were positive for metastases according to histopathology. A total of 126 independent sites were marked for diagnosis; at 105 of these sites the image was correlated with the histopathological diagnosis. 242 distinct images with adjacent fields of view were collected at these 105 sites. Of these images, 150 were of normal lymphoid tissue and 92 were of sites with metastases. Table 1 shows the distribution of data.

#132359 - $15.00 USD Received 30 Jul 2010; revised 11 Sep 2010; accepted 11 Sep 2010; published 16 Sep 2010

Table 1. Distribution of Collected Data from 43 Axillary Lymph Nodes in 14 Breast Cancer Patients

	Histologically Normal	Histologically Metastatic	Total
Axillary Lymph Nodes	27	16	43
Independent Sites with Histological Diagnosis	71	34	105
Images from Adjacent Fields of View	150	92	242

Figure 2 contains an HRFM image in which both adipose and lymphoid tissue are visible [Fig. 2(a)]. Adipocytes display a characteristic lobular structure, while lymphocytes are very small and more densely packed. Figure 2(b) shows the green channel of the field that was used to calculate feature values; the region containing adipocytes is cropped out. Figure 2(c) is the corresponding histology image.

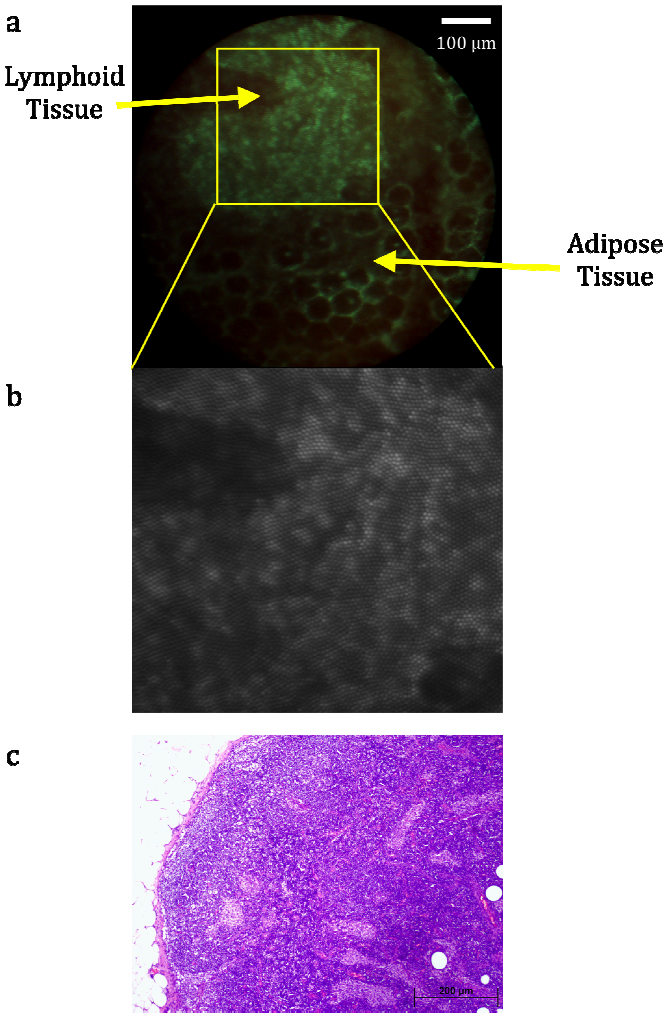

Fig. 2. (a) High-resolution fiber optic microscopy (HRFM) image taken with from a histologically normal lymph node in a region containing both adipocytes and lymphocytes after application of proflavine to highlight cell nuclei (b) Green channel of the image after cropping to remove adipocytes; quantitative features were calculated from this region (c) Corresponding histology at this site shows a normal lymph node. Capsule is thin and unremarkable. Fat surrounds the node. The node is populated with uniform, small, round lymphocytes.

#132359 - $15.00 USD Received 30 Jul 2010; revised 11 Sep 2010; accepted 11 Sep 2010; published 16 Sep 2010

Figure 3 illustrates representative results from a set of lymph nodes from a single patient. Figure 3(a) shows the photograph of three bisected nodes with eight imaging sites marked in blue for subsequent pathologic correlation. After examining the corresponding H&E slides, a dedicated breast pathologist determined that the node on the left was positive for metastases, with a negative periphery. The node in the middle was negative for metastases. Images collected from both of these nodes could be used in image analysis because the measurement site could be correlated to a histopathology gold standard. The node on the right was determined to be positive with very small subtle occasional single tumor cells with no dominant mass. Images from this node were not used in further analysis because it was difficult to determine if HRFM measured a site containing a few tumor cells or not. Figure 3(b) shows representative HRFM images collected at Sites 4 and 7 in the photograph. The HRFM image from site 7 has larger, more crowded nuclei and the average image intensity is greater as a result. The HRFM image from site 4 has smaller nuclei that are spaced farther apart; the average image intensity is lower because the cells are not as densely packed. The corresponding H&E images for these sites are shown in Fig. 3(c). The H&E image of site 7 indicates nests of tumor cells, while that of site 4 shows a normal node with sinus histiocytosis. Figure 3(d) depicts the image histograms that were obtained for each field shown in Fig. 3(b). The red histogram corresponds to the image obtained from site 7 (metastatic), while the blue histogram corresponds to the image obtained from site 4 (normal lymphoid tissue). Calculated feature values for each image are indicated. The metastatic site has a higher mean intensity than the normal site as seen by the shift in the center of the image histogram. Low skewness is noted in the metastatic site, indicating a more symmetrical histogram, while high skewness is noted in the normal site as a result of more pixel values concentrated at lower intensities with a long tail at higher intensity values. Kurtosis is higher for the normal site as seen by the sharp, high peak in the histogram, while the histogram of the metastatic site has a broader peak with lower kurtosis. The metastatic site has higher entropy, which indicates that the image is more random than the normal site. Standard deviation is higher in the metastatic site as seen by the wider distribution of pixel values around the mean as compared to the normal site.

#132359 - $15.00 USD Received 30 Jul 2010; revised 11 Sep 2010; accepted 11 Sep 2010; published 16 Sep 2010

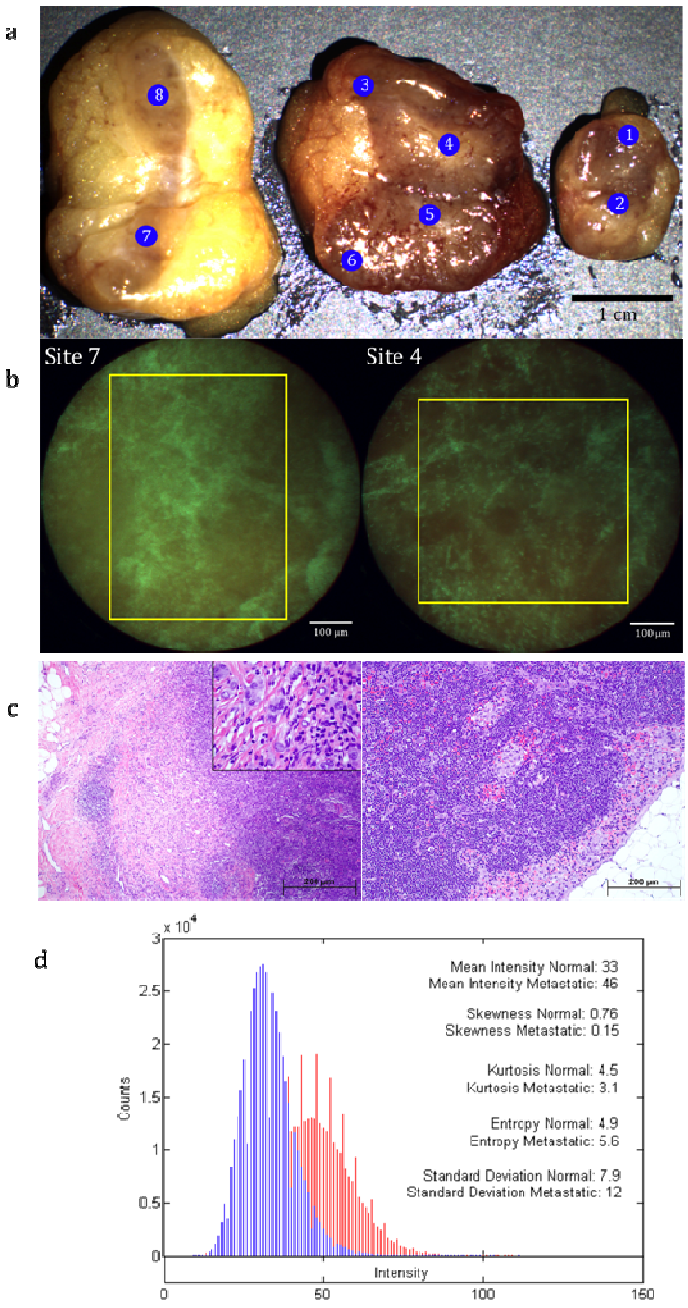

Fig. 3. (a) Photograph of three lymph nodes from a single patient with imaging sites marked in blue for correlation to pathology (b) HRFM images collected from sites 7 and 4 with cropped region of interest indicated: site 7 contains metastases while site 4 is normal lymphatic tissue (c) Corresponding H&E images for these sites: The image from site 7 shows that metastatic carcinoma has replaced part of the lymph node. Dense fibrosis surrounds the metastatic tumor cells. Insert shows high power magnification (40X) of tumor cells. The neoplastic cells are arranged in nests and have amphophilic, vacuolated cytoplasms and prominent nuclei. The image from site 4 shows a normal lymph node with sinus histiocytosis. The lymph node capsule is thin and the sub-capsular sinus contains reactive histiocytes. (d) Image histograms from each region of interest; site 7 is shown in red while site 4 is shown in blue. Calculated feature values for each image are also indicated.

#132359 - $15.00 USD Received 30 Jul 2010; revised 11 Sep 2010; accepted 11 Sep 2010; published 16 Sep 2010

Figure 4 shows box plots of the average feature values for each diagnostic category. Red boxes represent feature values from sites containing metastases, while blue boxes represent normal sites. All feature values were normalized to the median value of the normal lymphoid tissue set in order to show the range of values on a consistent scale. P-values from a one-way ANOVA test for each feature are also included in Fig. 4, and the features are listed in order from lowest p-value to highest. The average feature values of normal lymphoid tissue are statistically significantly different from the feature values of metastatic tissue for all five features ($p < 0.05$).

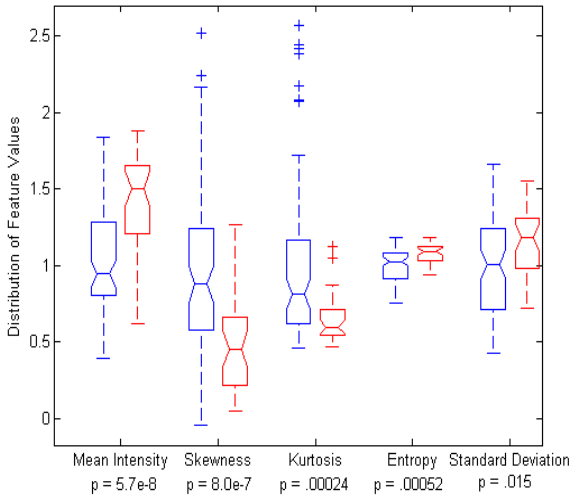

Fig. 4. Box plots showing feature values for images separated by diagnostic category. Values from images containing normal lymphatic tissue are shown in blue, while values from images containing metastases are red. All values are normalized to the median value of the normal set in order to show all features on the same scale. P-values obtained from a one-way ANOVA test are listed for each feature.

Table 2 ranks the diagnostic performance of each of the five image features by linear discriminant analysis, listed in order from highest to lowest AUC. Mean image intensity and skewness were the two highest performing features, each with an AUC of 0.81. This order of performance is consistent with the p-values for each feature (Fig. 4).

Table 2. Feature Performance

	Quantitative Feature	Sensitivity	Specificity	AUC
1	Mean image intensity	82% (28/34)	69% (49/71)	0.81
2	Skewness	85% (29/34)	66% (47/71)	0.81
3	Kurtosis	71% (24/34)	73% (52/71)	0.76
4	Entropy	59% (20/34)	76% (54/71)	0.70
5	Standard deviation	65% (22/34)	65% (46/71)	0.64

Figure 5 illustrates results when the top performing two individual features, mean image intensity and skewness, were combined. Figure 5(a) shows a scatter plot of mean intensity versus skewness for each image; both features provide discriminatory ability. Figure 5(b) shows the ROC curve for the algorithm developed using both features. The resulting AUC improved to 0.84. At the Q-point of the ROC curve, sensitivity and specificity with this two-feature algorithm were 79% (27/34) and 77% (55/71), respectively. An AUC value of 0.85 was obtained when the data were randomly divided into training and test groups by patient, with all images from a specific patient assigned to either testing or training. This simulates the process of collecting a training group to train the algorithm, and then collecting a separate patient set for testing, so it is encouraging that the performance is nearly identical to the results obtained when the entire data set was used for both training and testing. Although

#132359 - $15.00 USD Received 30 Jul 2010; revised 11 Sep 2010; accepted 11 Sep 2010; published 16 Sep 2010

performance of the algorithm could improve slightly if all five of the investigated features were used in combination, this would likely result in overtraining of the algorithm due to the small size of the data set from this pilot study, and so the algorithm was limited to only two combined features.

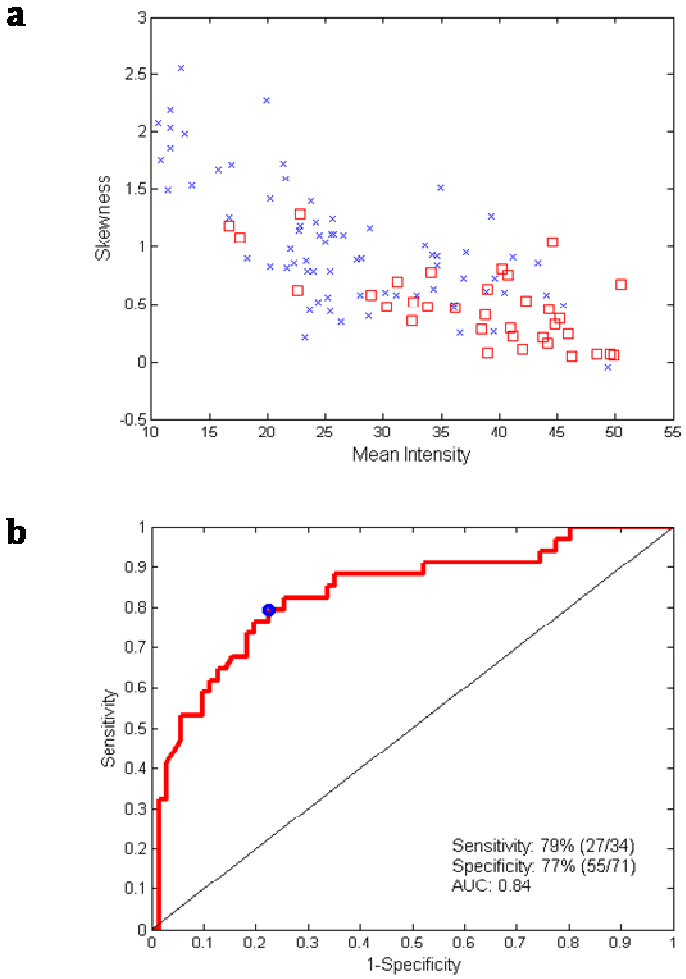

Fig. 5. (a) Scatter plot by site of mean intensity and skewness: normal sites are shown as a blue 'x' while metastatic sites are shown as a red square. (b) ROC curve obtained from a classification algorithm using linear discriminant analysis with both mean intensity and skewness as features

4. Discussion

This pilot study demonstrates the technical feasibility of *ex vivo* HRFM with proflavine contrast enhanced fluorescence imaging to visualize cell nuclei in axillary lymph nodes from breast cancer patients. These preliminary results demonstrate encouraging diagnostic potential of this fluorescence molecular imaging modality to identify lymph nodes containing metastases. Using the image features of mean intensity and skewness, a classification algorithm separating normal lymphoid tissue from tissue containing metastases was developed that could achieve an AUC of 0.84. This compares with the reported sensitivity and specificity of current standard preoperative sonographic methods of evaluating axillary nodes; a recent review of 16 published studies described sensitivity ranging between 49 and 87%, and specificity between 56 and 97% [21]. One comparative advantage of optical imaging is the

#132359 - $15.00 USD Received 30 Jul 2010; revised 11 Sep 2010; accepted 11 Sep 2010; published 16 Sep 2010

high resolution, which may make this technology more useful for detecting microscopic disease.

Differences observed in these image features are consistent with qualitative differences observed between images from normal lymphoid tissue and metastatic regions. Images obtained from metastatic sites appear brighter (higher mean image intensity) than images obtained from normal lymphoid tissue. This is due to the enlarged, crowded nuclei present in tumor cells, while normal lymphocytes have small nuclei that are spaced further apart. Higher mean intensity may also reflect the higher occurrence of diploidy and multiploidy and increased genetic material in cancer cells. Because images of normal lymph nodes have nuclei that are spaced further apart, there are more dark pixels, resulting in a positive skewness. Images of metastatic nodes have fewer low pixel values due to crowding and enlargement of nuclei and therefore have lower skewness. Calculations to determine mean intensity and skewness of an image can be performed extremely rapidly, potentially allowing a classification prediction in near real time. The step of cropping the image is critical for quality control, as acellular regions of fibrosis or folding of the tissue were occasionally observed to also display brighter fluorescence signal. This demonstrates why the high resolution imaging itself is important; simple intensity measurements would not be able to distinguish between tissue types. Though choosing a region that contains only nuclei could potentially introduce some user bias, this step prevents some false positive results.

While this pilot study demonstrates encouraging results regarding the technical feasibility of HRFM with proflavine to visualize cell nuclei in axillary lymph nodes from breast cancer patients and the diagnostic potential of HRFM with proflavine to differentiate benign from malignant axillary lymph nodes using quantitative image features of mean intensity and skewness, future studies are needed to evaluate the diagnostic performance of the imaging method in a larger, independent validation set of patients. Additional improvements to this technique include increasing the size of the fiber bundle to twice the current diameter, thereby increasing the field of view four-fold. Expanding the area that can be optically interrogated could improve the ability to detect metastatic cells by more efficiently imaging a lymph node with decreased imaging time. Future clinical studies will also attempt to determine the minimum size of metastasis that can be detected with this system.

The prognostic relevance of isolated tumor cells and micrometastases in lymph nodes from patients with breast cancer has become a major area of interest in tandem with the increased identification of this low volume disease due to the practice of SLN biopsy [22]. There is also heightened interest in the evaluation of the SLNs after neoadjuvant chemotherapy, where the proportion of micrometastases is reportedly higher, and the performance of intraoperative imprint cytology of SLNs is proportionately lower [23].

Many functional and molecular imaging techniques are being challenged to detect metastatic disease at the microscopic level in SLNs [24–26]. Noninvasive, non-ionizing, and high-resolution mapping of SLNs in conjunction with minimally invasive techniques, such as fine needle aspiration biopsy, is currently being investigated in multiple active preclinical protocols. While HRFM has good spatial resolution and high collection speed using current instrumentation, the current limitation for *in vivo* HRFM of lymph nodes is depth penetration. A potential resolution to this limitation is the in situ delivery of HRFM (i.e. endoscopy via a biopsy needle) for real-time *in vivo* interrogation of lymph nodes that are assessed preoperatively with ultrasound. The additional costs of performing imaging and imaging-guided biopsies may be balanced on average by cost savings from avoiding SLN evaluations for patients with documented nodal metastases preoperatively [27]. An aspect of this technique that may limit speed of translation to the clinic is the necessary approval process from the United States Food and Drug Administration (FDA) to use proflavine in human subjects. However, these pilot studies are necessary to provide the foundation for future pursuit of human trials. Optical imaging can be performed very rapidly, allowing a large area to be surveyed in a short time, making it an attractive technology for this application. An advantage of optical imaging over traditional histopathology is that this rapid imaging can be performed *in vivo*. However, the intent of this technology is to augment current standards of

#132359 - $15.00 USD Received 30 Jul 2010; revised 11 Sep 2010; accepted 11 Sep 2010; published 16 Sep 2010

care, not to attempt to replace the gold standard of histopathology. The role of HRFM in the future may be best suited for intra-operatively identifying candidates for full axillary dissection, thus preventing the need for a second surgery in some patients, or for preoperative staging of axilla.

These preliminary results demonstrate the technical feasibility and diagnostic potential of quantitative molecular imaging using HRFM with proflavine fluorescent staining to discriminate between normal and metastatic axillary lymph nodes *ex vivo* in breast cancer patients. This rapid technique is simple, inexpensive, and can potentially be exploited to augment patient care by providing an alternative technique for the detection of micrometastases while requiring fewer resources and expertise.

Acknowledgments

Funded by Career Development Award of Breast SPORE Grant no. 5P50 CA116199. This material is also based on work supported by the National Institutes of Health under grant no. 5T32 GM008362. The project described was also supported by the National Institutes of Health under grant Number R01EB007594. Its contents are solely the responsibility of the authors and do not necessarily represent the official views of the RCE Programs Office or NIH.

#132359 - $15.00 USD Received 30 Jul 2010; revised 11 Sep 2010; accepted 11 Sep 2010; published 16 Sep 2010